extinction coefficient of rhodopsin, γ is the quantum efficiency of bleaching, I_0 is the photon flux at the base of the ROS, and t is the duration of light exposure. For the derivation of Eq. 1, it was assumed that the light destroyed the pigment and that the pigment did not diffuse through the medium. The region below the curve represents the distribution of rhodopsin that was not bleached during the light exposure, whereas the region above represents the pattern of bleaching.

These measurements reveal the way in which toad ROSs receive the light stimulus in situ. A photon absorbed by a rhodopsin molecule results in the localized closure of Na^+ channels at the plasmalemma; one photon results in the closure of the channels in a ring around the rhodopsin that absorbed it (*18, 19*). As the light intensity increases, more rings of plasmalemma are recruited. The model for the spatial pattern of bleaching, as stated in Eq. 1, helps to quantify the recruitment aspect of the photoreceptor cell response. It may then become possible to predict the responsivities of single rod photoreceptor cells during illlumination through the intact physiological optics of the eye.

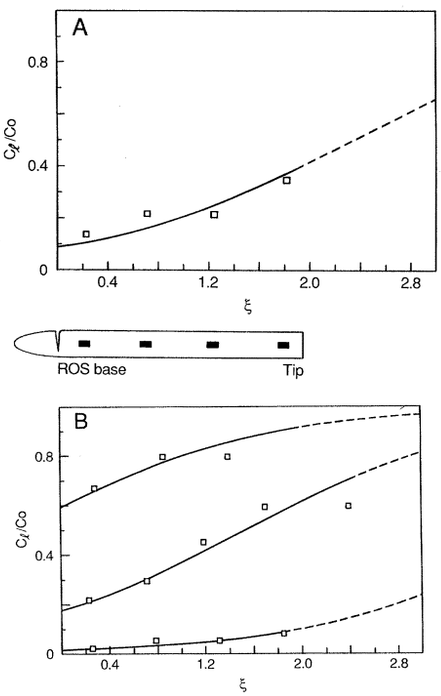

Fig. 2. Fraction of rhodopsin remaining as a function of ξ. The data are plotted as squares. The lines represent the best fits to Eq. 1. The lines are continuous to the end of the ROS; broken line extensions are included for illustrative purposes. (**A**) Each square represents a curve from Fig. 1, plotted here in terms of the fraction of the dark-adapted rhodopsin content remaining as a function of $\xi = \alpha c_0 l$, normalized distance from the base. In the ROS drawn beneath the graph, filled rectangles show where the absorbance spectra were measured. The photon dosage received by the ROS was 1.49×10^8 photons per square micrometer (*20*). (**B**) The bleaching patterns after light exposures of different strengths are illustrated by the results from three ROSs. From the top curve downward, the photon dosages were 3.26×10^7, 1.07×10^8, and 2.59×10^8 photons per square micrometer (*20*), respectively.

REFERENCES AND NOTES

1. A. Laties, *Tissue Cell* **1**, 63 (1969).
2. ——— and J. M. Enoch, *Invest. Ophthalmol.* **10**, 69 (1971).
3. N. G. Webb, *Nature (London)* **235**, 44 (1972).
4. S. V. G. Nilsson, *J. Ultrastruct. Res.* **10**, 390 (1964).
5. P. A. Liebman and G. Entine, *Science* **185**, 457 (1974).
6. M.-m. Poo and R. A. Cone, *Nature (London)* **247**, 438 (1974).
7. R. A. Cone, *Nature (London) New Biol.* **236**, 39 (1972).
8. P. K. Brown, *ibid.*, p. 35.
9. J. J. Wolken, *J. Opt. Soc. Am.* **53**, 1 (1963); P. A. Liebman, *Biophys. J.* **2**, 161 (1962).
10. The Ringer solution contained 100 m*M* NaCl, 11.9 m*M* $NaHCO_3$, 3.3 m*M* $NaHPO_4$, 2.5 m*M* KCl, 3.0 m*M* $MgCl_2$, and 10.0 m*M* glucose.
11. The light from a Bausch and Lomb monochromator was focused onto a diffusing plate. The diffusing plate was a sheet of 1/4-inch sandblasted plexiglass.
12. G. Wald and R. Hubbard, *Proc. Natl. Acad. Sci. U.S.A.* **36**, 92 (1950).
13. M. Zewi, *Acta Soc. Sci. Fenn. Nova Ser. B* **2**, 1 (1939).
14. R. Hoffman and S. F. Basinger, *Vision Res.* **17**, 335 (1977).
15. D. Mazia, G. Schatten, W. Sale, *J. Cell Biol.* **66**, 198 (1975).
16. E. F. MacNichol, in *Frontiers in Visual Science, Proceedings of the University of Houston College of Optometry Dedication Symposium, Houston, Texas, March 1977*, S. J. Cool and E. L. Smith III, Eds., vol. 8 of Springer Series in Optical Sciences (Springer-Verlag, New York, 1978), pp. 194–208.
17. B. Rabinovitch, *Photochem. Photobiol.* **17**, 479 (1973).
18. W. A. Hagins, R. D. Penn, S. Yoshikami, *Biophys. J.* **10**, 380 (1970).
19. P. A. McNaughton, K.-W. Yau, T. D. Lamb, *Nature (London)* **283**, 85 (1980).
20. The fit of the data to Eq. 1 was used to generate the value for photon dosage ($I_0 t$) received by each ROS. The data shown are representative of 129 measurements made on 37 ROSs, with photon dosages ranging up to 2.76×10^8 photons per square micrometer.

21. We wish to thank D. A. Baylor and T. A. Hume for help in the manuscript preparation and B. J. Williams for the illustrations. Supported by a grant from the Robinson Neurological Foundation and by NSF grant BNS 84-11971.

1 July 1987; accepted 28 October 1987

A Novel Putative Tyrosine Kinase Receptor Encoded by the *eph* Gene

HISAMARU HIRAI,* YOSHIRO MARU, KOICHI HAGIWARA, JUNJI NISHIDA, FUMIMARO TAKAKU

Growth factors and their receptors are involved in the regulation of cell proliferation and also play a key role in oncogenesis. In this study, a novel putative kinase receptor gene, termed *eph*, has been identified and characterized by molecular cloning. Its primary structure is similar to that of tyrosine kinase receptors thus far cloned and includes a cysteine-rich region in the extracellular domain. However, other features of the sequence distinguish the *eph* gene product from known receptors with tyrosine kinase activity. Thus the *eph* protein may define a new class of these molecules. The *eph* gene is overexpressed in several human carcinomas, suggesting that this gene may be involved in the neoplastic process of some tumors.

SEVERAL VIRAL ONCOGENES AND CELLULAR proto-oncogenes comprise a gene family whose products exhibit tyrosine-specific protein kinase activity and are associated with the plasma membrane (*1*). Such features are shared by several genes encoding polypeptide hormone receptors, including epidermal growth factor receptor (EGF-R-1)/c-*erb*B (*2*), EGF-R–related receptor (EGF-R-2)/*neu*/*erb*B-2 (*3*), insulin receptor (IR) (*4*), insulin-like growth factor–I receptor (IGF-I-R) (*5*), platelet-derived growth factor receptor (PDGF-R) (*6*), and colony-stimulating factor–1 receptor (CSF-1-R)/c-*fms* (*7*). In addition, several viral oncogenes appear to encode mutated tyrosine kinase receptors whose cellular homologs have not yet been identified. The importance of tyrosine kinase activity in both normal and abnormal growth regulation suggests that additional tyrosine kinases also exist.

We searched a human genomic library for gene sequences homologous to the tyrosine kinase domain of the viral oncogene v-*fps* (legend to Fig. 1A). A 12.5-kb Eco RI fragment (Cl-7) was found to be homologous to the v-*fps* probe under relaxed hybridization conditions (Fig. 1A). The 0.6-kb Hind III–Sst I fragment (HS fragment) from Cl-7, including the sequence homologous to the v-*fps* probe, was used as a probe in subsequent hybridization experiments. In an erythropoietin-producing human hepatocellular carcinoma cell line (ETL-1), the

The Third Department of Internal Medicine, Faculty of Medicine, University of Tokyo, Hongo, Tokyo 113, Japan.

*To whom correspondence should be addressed at Department of Microbiology and Immunology, Room HSE 411, University of California, San Francisco, CA 94143.

novel gene, which we have termed *eph*, is overexpressed 10- to 20-fold but not amplified (Fig. 1, B and C). Since the hybridization conditions were sufficiently stringent to avoid detection of the c-*fps* gene with the HS probe, all intense bands shown in Fig. 1C represent DNA fragments specific to the *eph* gene. The HS probe hybridized specifically to DNA fragments isolated from chicken, mouse, rat, and human cell types, and so we conclude that the *eph* gene has been highly conserved during vertebrate evolution.

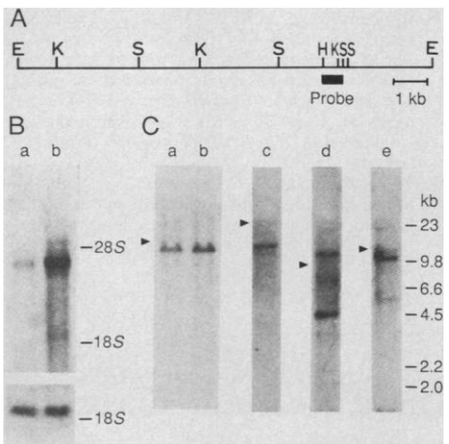

Fig. 1 Analysis of the *eph* gene. (**A**) Restriction map of the genomic clone Cl-7. E, S, K, and H represent restriction sites of Eco RI, Sst I, Kpn I, and Hind III, respectively. The thick bar indicates the HS fragment. A human genomic library was constructed from placental DNA with λgt·WES·λB phage vector as described (*21*). This library was screened with a 0.4-kb Bam HI fragment of v-*fps* DNA (*13*). Plaque hybridization was carried out in 30% formamide, 5× Denhardt's solution, 5× SSPE (0.15*M* NaCl, 0.01*M* NaH_2PO_4, and 0.001*M* EDTA), 0.1% SDS, and denatured salmon sperm DNA (100 μg/ml) for 20 hours at 42°C. (**B**) Northern blot analysis of the *eph* transcript. Polyadenylated RNAs (5 μg per lane) from normal human liver (lane a) and ETL-1 cell line (lane b) were hybridized with the HS probe (upper) and with the β-actin probe (*22*) (lower). Total RNA was extracted by the guanidine isothiocyanate–cesium chloride method (*23*). Polyadenylated RNAs selected by oligo(dT)-cellulose (*24*) were separated on a formaldehyde-containing 1% agarose gel (*25*). The RNAs were transferred to a nylon membrane (*26*) and hybridized in 50% formamide, 5× standard saline citrate, denatured salmon sperm DNA (100 μg/ml), 10× Denhardt's solution, 0.1% SDS, 10% dextran sulfate, and the HS probe for 20 hours at 42°C. Hybridization was detected by autoradiography. The washed filter was reused in hybridization with the actin probe. (**C**) Southern blot analysis of the genomic *eph* gene. DNAs prepared from normal human placenta (lane a), ETL-1 cells (lane b), chicken liver (lane c), mouse liver (lane d), and rat liver (lane e) were hybridized with the HS probe. Arrows indicate positions of c-*fps* fragments that hybridized with the original v-*fps* probe under the same conditions. High molecular weight DNAs (10 μg per lane) were digested with Eco RI, separated by electrophoresis through 0.8% agarose gels, and blotted to nylon membranes (*27*). Hybridization conditions were as described for (B).

These conclusions were confirmed with the complementary DNA (cDNA) probe described below (*8*).

Two cDNA libraries constructed from ETL-1 messenger RNA (mRNA) were screened with the HS probe. Three of 24 isolated clones contained inserts of 3.5 kb, which is large enough to represent all or nearly all of the 3.5-kb *eph* mRNA. Detailed restriction maps were identical between two cDNA clones (Cl-70 and Cl-73) that were independently isolated from each of the two cDNA libraries. We used Cl-70 in all subsequent studies. In Northern blot hybridization, CL-70 cDNA reacted with a 3.5-kb mRNA detected by the HS probe and with no additional transcripts (*8*).

The complete nucleotide sequence of the

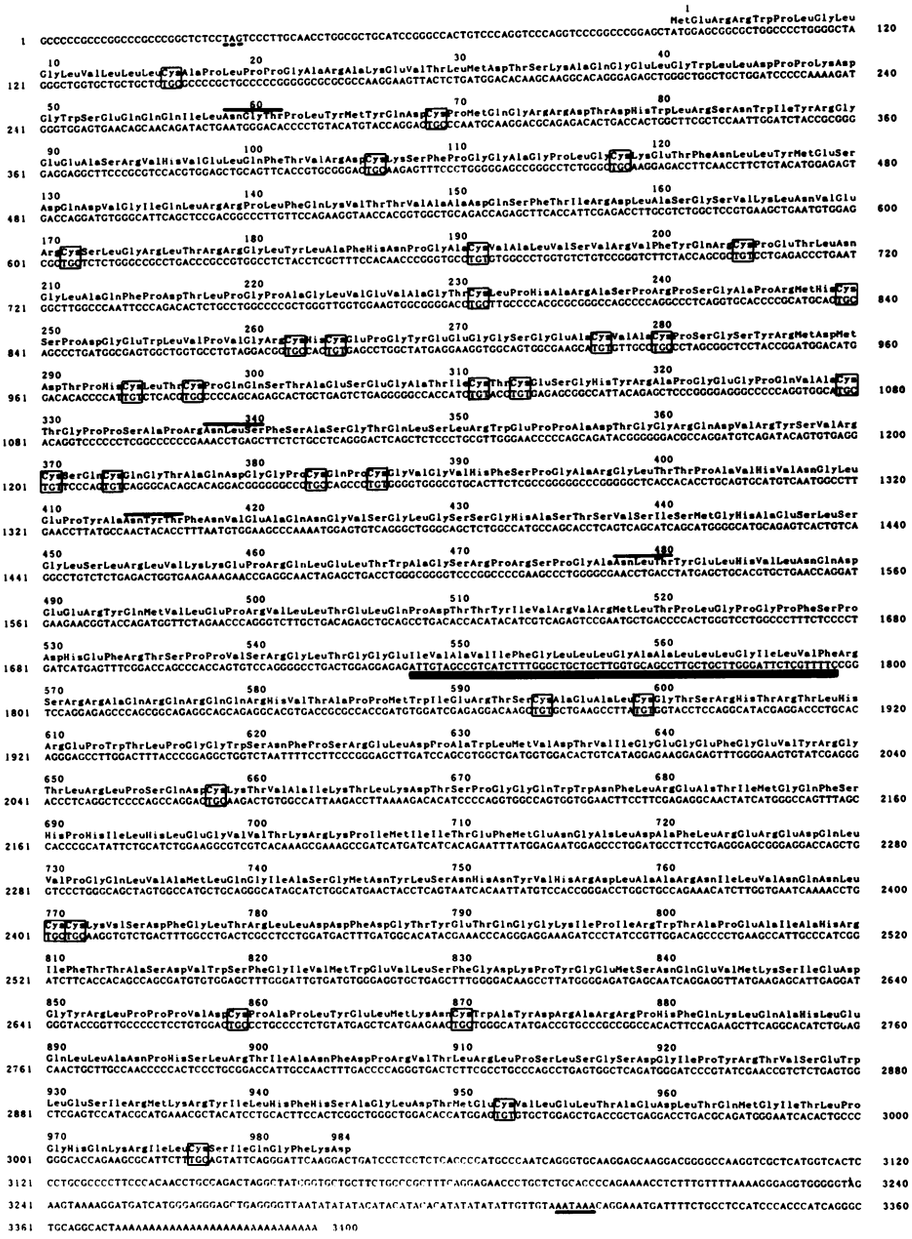

Fig. 2. Complete nucleotide and amino acid sequence of the *eph* cDNA. Nucleotides are numbered at both sides. Amino acids are numbered above the sequence, starting with the initiation methionine. A heavy black bar demarcates the putative transmembrane region. Potential sites of *N*-linked glycosylation are overlined. The AATAAA consensus sequence near the polyadenylated 3′ end of the cDNA is underlined. All cysteine residues are boxed. A broken underline indicates an in-frame stop codon in the 5′-untranslated region. Polyadenylated RNA was prepared from ETL-1 cells (legend to Fig. 1B). Two cDNA libraries were independently constructed with the λgt10 vector (*28*). Total 4×10^5 independent clones were screened with the HS probe. Hybridization was carried out at 42°C for 20 hours under stringent conditions [50% formamide, 5× Denhardt's solution, 5× SSPE, 0.1% SDS, and denatured salmon sperm DNA (100 μg/ml)]. Nucleotide sequence analysis was performed by subcloning of restriction fragments of the clone Cl-70 DNA into M13 cloning vectors, followed by primed DNA synthesis on single-stranded DNA templates in the presence of dideoxynucleotide triphosphates (*29*).

Cl-70 cDNA insert extends for 3400 nucleotides and contains a single long open reading frame of 2952 nucleotides, encoding a putative primary translation product of 984 amino acids (relative molecular mass 108,801) (Fig. 2). A polyadenylation signal (AATAAA) is found 49 nucleotides upstream from a polyadenylate sequence at the 3′ end of the cDNA. Although the flanking nucleotides of the predicted initiation codon ATG are not a perfect match with the consensus for a translation initiation site (*9*), we believe that this codon is the initiation codon because an in-frame stop codon can be identified in the 5′-untranslated region (Fig. 2). Furthermore, most of the first 23 amino acid residues are highly hydrophobic, suggesting that they represent the signal peptide sequence necessary for transport of the nascent polypeptide chain into the lumen of the endoplasmic reticulum (*10*). In addition to the signal sequence, the deduced 984–amino acid polypeptide sequence contains the features characteristic of cell surface receptors. These include a stretch of 21 hydrophobic amino acids (residues 548 to 568) characteristic of a membrane-anchoring domain. This sequence is flanked on its carboxyl side by a basic sequence (Arg-Ser-Arg-Arg) typical for the junction between the membrane and cytoplasmic domains of cell surface receptors (*2–7*). All four possible *N*-linked glycosylation sites are distributed in the putative extracellular half of the sequence (Fig. 2). Eighteen of a total of 31 cysteine residues are found clustered near the middle portion (residues 171 to 386) of the presumptive extracellular domain (Fig. 2). Similarly, EGF-R-1 has two cysteine-rich regions (residues 161 to 342 and 500 to 636), which contain 25 and 21 cysteine residues, respectively, and 27 cysteine residues are clustered between residues 148 and 323 of IR (*2, 4*).

The sequence of 245 amino acids between residues 638 and 882 includes the residues possibly involved in adenosine triphosphate binding (residues 640, 642, 645, and 664) and a tyrosine residue (residue 789) homologous to the major autophosphorylation site (Tyr^{416}) in $pp60^{v\text{-}src}$ (*11*). This domain is homologous with retroviral oncogene products of the *src* family (v-*yes*, 47%; v-*src*, 46%; v-*fgr*, 45%; v-*abl*, 44%; v-*fps*, 43%; v-*ros*, 41%; v-*erb*B, 40%; v-*fms*, 38%; and v-*kit*, 37%) (*12–14*) and with tyrosine kinase receptor sequences (IR, 41%; EGF-R-1, 41%; EGF-R-2, 40%; IGF-I-R, 39%; PDGF-R, 38%; and CSF-1-R, 37%) (*2–7*). Further, the amino acid sequence is homologous with that of the corresponding portion of *met*, *trk*, c-*ros*, and *ret* (36 to 40% homology) (*15*). These relations strongly suggest that the *eph* protein has tyrosine kinase activity. From these observations, we tentatively conclude that the *eph* gene product is a transmembrane glycoprotein that may act as a receptor for a growth factor.

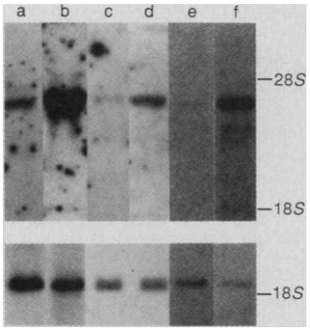

Fig. 3. The *eph* transcript in fresh human carcinomas. Five micrograms of polyadenylated RNAs from normal colon (lane a), colon carcinoma (lane b), normal lung (lane c), lung adenocarcinoma (lane d), normal mammary gland (lane e) and mammary carcinoma (lane f) were hybridized with the *eph* cDNA probe (the total insert DNA of Cl-70) (upper) and with the β-actin cDNA probe (lower). Hybridization conditions were as described in the legend to Fig. 1B.

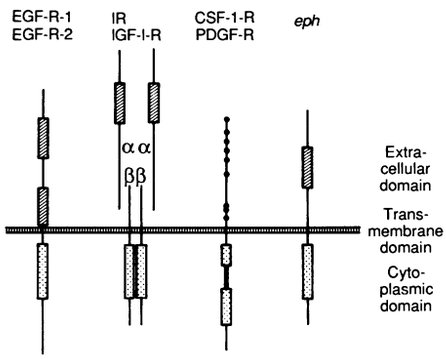

Fig. 4. Topological comparison of the *eph* protein and three types of tyrosine kinase receptors (*2–7*). Cysteine-rich regions are shown as hatched boxes. The distribution of cysteine residues in the extracellular domains of PDGF-R and CSF-1-R is indicated by closed circles. Tyrosine kinase domains are shown by shaded boxes. A heavy solid line indicates a stretch of sequence inserted within the tyrosine kinase domains of PDGF-R and CSF-1-R.

Several oncogenes encode mutated versions of receptors for growth factors, including v-*erb*B [truncated EGF-R-1 (*16*)], *neu* [mutated EGF-R-2 (3)], v-*fms*, [altered CSF-1 receptor (*17*)], and v-*ros* [IR-related (*4*)]. Evidence is accumulating that quantitative or qualitative mutations of proto-oncogenes (or both), can lead to cell transformation and can play a role in the neoplastic process of human tumors (*18*). For example, overexpression of the EGF-R-1 gene or the EGF-R-2 gene has been observed in a variety of human tumors (*2, 3, 19*). To determine if *eph* gene expression is altered in neoplastic tissues, we analyzed RNA from approximately 50 human tumors by Northern blotting. Overexpression of the *eph* gene was observed in several carcinomas, including colon carcinoma, lung adenocarcinoma, mammary carcinoma (Fig. 3), and hepatocellular carcinoma (Fig. 1). These observations suggest that elevated expresion of *eph* may provide a selective advantage in the process of carcinogenesis.

Common structural features of the *eph* gene product and tyrosine kinase receptors include a single stretch of hydrophobic amino acids representing a transmembrane sequence, an amino-terminal extracellular domain that presumably forms the ligand-binding pocket, and an intracellular domain that includes sequences specifying the tyrosine-specific protein kinase activity. In tyrosine kinase receptors thus far cloned, distinctive structural characteristics have suggested at least three classes of receptor: EGF-R-1 and EGF-R-2 as type 1, IR and IGF-I-R as type 2, and PDGF-R and CSF-1-R as type 3 (*20*). The *eph* protein has only one cysteine-rich region, unlike EGF-R-1 (*2*) and EGF-R-2 (*3*). It does not appear to contain the putative cleavage site of the proreceptor polypeptide, which is found in IR (*4*) and IGF-I-R (*5*), and it does not contain the insertion sequence that interrupts the tyrosine kinase domain of PDGF-R (*6*) and CSF-1-R (*7*) (Fig. 4). Therefore, the *eph* protein may define a fourth class of receptors with tyrosine kinase activity.

REFERENCES AND NOTES

1. T. Hunter and J. A. Cooper, *Annu. Rev. Biochem.* **54**, 897 (1985).
2. A. Ullrich *et al.*, *Nature (London)* **309**, 418 (1984).
3. L. Coussens *et al.*, *Science* **230**, 1132 (1986); C. I. Bargmann, M.-C. Hung, R. A. Weinberg, *Nature (London)* **319**, 226 (1986); T. Yamamoto *et al.*, *ibid.*, p. 230; C. I. Bargmann, M.-C. Hung, R. A. Weinberg, *Cell* **45**, 649 (1986).
4. A. Ullrich *et al.*, *Nature (London)* **313**, 756 (1985); Y. Ebina *et al.*, *Cell* **40**, 747 (1985).
5. A. Ullrich *et al.*, *EMBO J.* **5**, 2503 (1986).
6. Y. Yarden *et al.*, *Nature (London)* **323**, 226 (1986).
7. L. Coussens *et al.*, *ibid.* **320**, 277 (1986).
8. H. Hirai *et al.*, unpublished observations.
9. M. Kozak, *Nucleic Acids Res.* **9**, 5233 (1981).
10. G. Blobel, *Proc. Natl. Acad. Sci. U.S.A.* **77**, 1496 (1980); M. E. E. Watson, *Nucleic Acids Res.* **12**, 5145 (1984).
11. T. Takeya and H. Hanafusa, *Cell* **32**, 881 (1983).
12. A. P. Czernilofsky *et al.*, *Nature (London)* **287**, 198 (1980).
13. M. Shibuya and H. Hanafusa, *Cell* **30**, 787 (1982).
14. A. Hampe, M. Gobet, C. J. Sherr, F. Galibert, *Proc. Natl. Acad. Sci. U.S.A.* **81**, 85 (1984); N. Kitamura, A. Kitamura, K. Toyoshima, Y. Hirayama, M. Yoshida, *Nature (London)* **297**, 205 (1982); G. Naharro, K. C. Robbins, E. P. Reddy, *Science* **223**, 63 (1984); E. P. Reddy, M. J. Smith, A. Srinivasan, *Proc. Natl. Acad. Sci. U.S.A.* **80**, 3623 (1983); T. Yamamoto *et al.*, *Cell* **35**, 71 (1983); W. Neckameyer and L. H. Wang, *J. Virol.* **53**, 879 (1985); P. Besmer *et al.*, *Nature (London)* **320**, 415 (1986).
15. M. Dean *et al.*, *Nature (London)* **318**, 385 (1985); D. Martin-Zanca, S. H. Hughes, M. Barbacid, *ibid.* **319**, 743 (1986); W. S. Neckameyer, M. Shibuya, M. T. Hsu, L. H. Wang, *Mol. Cell. Biol.* **6**, 1478 (1986); M. Takahasi and G. F. Cooper, *ibid.* **7**, 1378 (1987).
16. J. Downward *et al.*, *Nature (London)* **307**, 521 (1984).

17. C. J. Sherr *et al.*, *Cell* **41**, 665 (1985).
18. G. Klein and E. Klein, *Nature (London)* **315**, 190 (1985); J. M. Bishop, *Science* **235**, 305 (1987).
19. T. A. Libermann *et al.*, *Nature (London)* **313**, 144 (1985); T. Yamamoto *et al.*, *Cancer Res.* **46**, 414 (1986); D. J. Slamon *et al.*, *Science* **235**, 177 (1987); M. H. Krans *et al.*, *EMBO J.* **6**, 605 (1987).
20. A. Ullrich *et al.*, *Cold Spring Harbor Symp. Quant. Biol.* **51**, 713 (1986).
21. H. Hirai *et al.*, *Blood* **66**, 1371 (1985).
22. D. W. Cleveland *et al.*, *Cell* **20**, 95 (1980).
23. J. M. Chirgwin, A. E. Przybyla, R. J. MacDonald, W. J. Ruffer, *Biochemistry* **18**, 5294 (1979).
24. H. Aviv and P. Leder, *Proc. Natl. Acad. Sci. U.S.A.* **69**, 1408 (1972).
25. H. Lehrach, D. Diamond, J. M. Wozney, H. Boedtker, *Biochemistry* **16**, 4743 (1977).
26. P. S. Thomas, *Proc. Natl. Acad. Sci. U.S.A.* **77**, 5201 (1980).
27. E. M. Southern, *J. Mol. Biol.* **98**, 503 (1975).
28. T. Huynh, R. Young, R. Davis, in *Practical Approaches in Biochemistry*, D. Grover, Ed. (IRL, Oxford, 1984), pp. 49–78.
29. F. Sanger, S. Nicklen, A. R. Coulson, *Proc. Natl. Acad. Sci. U.S.A.* **74**, 5463 (1977); J. Messing and J. Viera, *Gene* **129**, 269 (1982); J. Messing, R. Crea, P. H. Seeburg, *Nucleic Acids Res.* **9**, 309 (1981).
30. We thank H. E. Varmus and D. Morgan for comments on the manuscript. This work was supported in part by Grants-in-Aid for Cancer Research from the Ministry of Health and from the Ministry of Education, Science and Culture of Japan.

15 June 1987; accepted 22 October 1987

Sodium-Calcium Exchange in Heart: Membrane Currents and Changes in $[Ca^{2+}]_i$

L. BARCENAS-RUIZ, D. J. BEUCKELMANN, W. G. WIER

Recordings have been made of changes in intracellular calcium ion concentration ($[Ca^{2+}]_i$) that can be attributed to the operation of an electrogenic, voltage-dependent sodium-calcium (Na-Ca) exchanger in mammalian heart cells. Guinea pig ventricular myocytes under voltage clamp were perfused internally with fura-2, a fluorescent Ca^{2+}-indicator, and changes in $[Ca^{2+}]_i$ and membrane current that resulted from Na-Ca exchange were identified through the use of various organic channel blockers and impermeant ions. Depolarization of cells elicited slow increases in $[Ca^{2+}]_i$, with the maximum increase depending on internal $[Na^+]$, external $[Ca^{2+}]$, and membrane voltage. Repolarization was associated with net Ca^{2+} efflux and a decline in the inward current that developed instantaneously upon repolarization. The relation between $[Ca^{2+}]_i$ and current was linear, and the slope was made steeper by hyperpolarization.

THE EXISTENCE OF A SODIUM-CALCIUM (Na-Ca) exchanger has been established in many tissues (*1*), including intact heart tissue (*2*) and cardiac sarcolemmal vesicles (*3*). Experiments on single isolated heart cells from frog atria (*4*) and guinea pig ventricles (*5*) revealed currents that have been attributed to Na-Ca exchange. The role of Na-Ca exchange in the arrhythmogenic currents that accompany spontaneous fluctuations in intracellular calcium ion concentration ($[Ca^{2+}]_i$) (*6, 7*) has been shown (*8*), but $[Ca^{2+}]_i$ was not measured or controlled adequately in these studies. When recording the Ca^{2+}-activated fluorescence of fura-2 (*9*) in cardiac cells under voltage clamp (*10*), we observed that changes in fluorescence could be detected under conditions in which changes in $[Ca^{2+}]_i$ might be attributable to Na-Ca exchange. We now report (*11*) simultaneous measurements of changes in $[Ca^{2+}]_i$ and membrane current (*4, 5*), which we suggest are probably due to Na-Ca exchange.

The methods for voltage clamp preparation of single cells and for the recording of fura-2 fluorescence were similar to those described (*7, 10*). The cells were internally perfused over 5 to 15 minutes with a micropipette electrode (1.8 to 3.5 MOhm) filled with 0.070 m*M* fura-2 (Molecular Probes), 130 m*M* CsCl, 2 m*M* $MgCl_2$, 2 m*M* adenosine 5′-triphosphate (sodium salt), 0 to 10 m*M* NaCl, and 10 m*M* Hepes (potassium or sodium salt) (*p*H 7.2). (The $[Na^+]$ in the micropipette is indicated.) The cells were superfused at room temperature (23°C) with a physiological saline solution containing 2.5 m*M* $CaCl_2$, 135 m*M* NaCl, 10 m*M* CsCl, 1 m*M* $MgCl_2$, 0.33 m*M* NaH_2PO_4, 10 m*M* dextrose, 10 m*M* Hepes, 10 m*M* tetraethylammonium (TEA), 10 μ*M* verapamil, and 10 μ*M* ryanodine; *p*H was 7.3 with the addition of NaOH. Interfering potassium (K^+) currents were blocked by substituting impermeant ions (Cs^+ and TEA). Verapamil and ryanodine (*12*) blocked the interfering changes in $[Ca^{2+}]_i$ that result from entry of Ca^{2+} through surface membrane Ca^{2+} channels (*13*) or from release of Ca^{2+} from the sarcoplasmic reticulum (SR), respectively.

From a holding potential of −80 mV, depolarization for 1.5 seconds was associated with a slow increase in $[Ca^{2+}]_i$ (Fig. 1). As the membrane was depolarized more, the change in $[Ca^{2+}]_i$ became larger and faster. The $[Ca^{2+}]_i$ at the end of the depolarizing pulse increased monotonically with clamp-pulse potential (Fig. 1B). In Ca^{2+}-free solution, these changes did not occur. This is evidence for a voltage-dependent process that controls $[Ca^{2+}]_i$ in cells in which Ca^{2+} entry through channels and Ca^{2+} release from SR are blocked.

Repolarization to −80 mV was associated with the instantaneous development of a large inward current and the initiation of the decline in $[Ca^{2+}]_i$. Throughout the decline in $[Ca^{2+}]_i$, the current was directly proportional to $[Ca^{2+}]_i$ (Fig. 1C). At −80 mV, all ordered pairs ($[Ca^{2+}]_i$, current) fall on the same line independent of time or previous history of depolarization.

In the working scheme of electrogenic Na-Ca exchange (*14*), which we will use here, the exchange current (Eq. 3) is proportional to the difference between Ca^{2+} influx and efflux, where each unidirectional

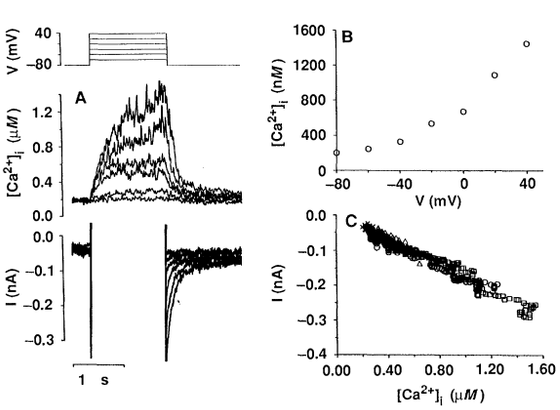

Fig. 1. Changes in $[Ca^{2+}]_i$ and membrane current attributed to Na-Ca exchange in a single guinea pig ventricular myocyte under voltage clamp. All data are from one representative cell, W74, of five cells studied with this protocol. Micropipette $[Na^+]$ was 7.5 m*M*. (**A**) Simultaneous recordings of $[Ca^{2+}]_i$ and membrane current. The holding potential was −80 mV, and depolarizing pulses lasting for 1.5 seconds were given from −60 to +40 mV. Outward currents during the depolarizing pulse are off-scale. (**B**) Voltage dependence of the change in $[Ca^{2+}]_i$. Values plotted are the average $[Ca^{2+}]_i$ over the last 200 msec of the depolarizing pulse. (**C**) The relationship between $[Ca^{2+}]_i$ and membrane current after repolarization. The current, *I*, has been plotted as a function of $[Ca^{2+}]_i$ at 2 msec intervals during the first second after repolarization from +40 mV (squares), +20 mV (circles), 0 mV (triangles), −20 mV (diamonds), and −40 mV (crosses).

Department of Physiology, University of Maryland School of Medicine, Baltimore, MD.